Molecular network analyses implicate death-associated protein kinase 3 (DAPK3) as a key factor in colitis-associated dysplasia progression

Huey-Miin Chen, PhD[1] and Justin A. MacDonald, PhD[1,*]

[1]Department of Biochemistry & Molecular Biology, Cumming School of Medicine, University of Calgary, 3280 Hospital Drive NW, Calgary, AB, T2N 4Z6, Canada

* **Correspondence to**: Justin MacDonald, Department of Biochemistry & Molecular Biology, University of Calgary, 3280 Hospital Drive NW, Calgary, AB, T2N 4Z6. Tel: 403-210-8433; Email: jmacdo@ucalgary.ca

Funding Disclosure: This work was supported by a research grant from the Canadian Institutes of Health Research (MOP#97931 to J.A.M.). H.-M.C. was recipient of CIHR Fredrick Banting and Charles Best Canada and Alberta Graduate Excellence Scholarships.

Authors' Financial Disclosure and Conflicts of Interest: J.A.M. is cofounder and has an equity position in Arch Biopartners Inc. All other authors declare no conflicts of interest.

Summary: Our investigation verified pancolitis as a conduit for UC advancement from left-sided colitis to dysplasia and uniquely identified dysregulation of actin reorganization with DAPK3 and YAP as key molecular determinants for disease progression.

ABSTRACT

Background Ulcerative colitis (UC) is a progressive disorder that elevates the risk of colon cancer development through a colitis-dysplasia-carcinoma sequence. Gene expression profiling of colitis-associated lesions obtained from patients with varied extent of UC can be mined to define molecular panels associated with colon cancer development. *Methods* Differential gene expression (DEGs) profiles of three UC clinical subtypes and healthy controls were developed for the GSE47908 microarray dataset of healthy controls, left-sided colitis, pancolitis, and colitis-associated dysplasia (CAD) using limma R. *Results* Gene ontology (GO) enrichment analysis of DEGs revealed a shift in transcriptome landscape as UC progressed from left-sided colitis to pancolitis to CAD, from being immune-centric to being cytoskeleton-dependent. Hippo signaling (via Yes-associated protein, YAP) and Ephrin receptor signaling were the top canonical pathways progressively altered in concert with the pathogenic progression of UC. Molecular interaction network analysis of DEGs in left-sided colitis, pancolitis, and CAD revealed one pairwise line or *edge* that was topologically important to the network structure. This edge was found to be highly enriched in actin-based processes, and death-associated protein kinase 3 (DAPK3) was a critical member and sole protein kinase member of this network. DAPK3 is a regulator of actin-cytoskeleton reorganization that controls proliferation and apoptosis. Differential correlation analyses revealed a negative correlation for *DAPK3-YAP* in healthy controls which flipped to positive in left-sided colitis. With UC progression to CAD, the *DAPK3-YAP* correlation grew progressively more positive. *Conclusion* In summary, DAPK3 was identified as a candidate gene involved in UC progression to dysplasia.

KEY WORDS

death-associated protein kinase, zipper-interacting protein kinase, differential-gene expression, ulcerative colitis, dysplasia, colon cancer

KEY MESSAGES

- Ulcerative colitis (UC) patients have greater risk of developing colitis-associated colorectal cancer (CAC) with the evolutionary trajectory of disease initiated early in the colitis-dysplasia-carcinoma sequence.
- The dysregulation of actin reorganization, with DAPK3 and YAP involvement, was uniquely identified as a determinant for the progression of UC from non-dysplastic to dysplastic UC.
- Relevant gene expression changes occur before histological evidence of dysplasia/carcinoma, so the results could be exploited for the development of biomarkers that identify the risk of dysplasia progression for UC patients.

1. INTRODUCTION

Ulcerative colitis (UC) is a chronic, inflammatory bowel disease (IBD) that is confined to the mucosal layer of the large bowel, most commonly the rectum, and may extend proximally in a continuous fashion [1]. This is a heterogeneous and progressive disorder that has seen a substantial increase in global prevalence. The current framework of UC pathogenesis comprises environmental, genetic, immune, and microbiome factors that culminate at the perturbation of the mucosal barrier and prolonged mucosal inflammatory response [2]. Consequently, UC is a clinically-, molecularly-, and genetically- heterogeneous disease that fosters varied disease course and mixed response to therapy [3]. The genetic heterogeneity is highlighted in the analysis of 75,000 IBD cases and controls by Jostins and colleagues that identified 23 UC-specific risk loci with primary involvement in the regulation of epithelial barrier function and immune pathways [4]. Genetic studies such as this promote the concept that UC disease susceptibility is a compilation of small effects/gene-alterations that is not shared by all patients.

UC patients are at greater risk of developing colitis-associated colorectal cancer (CAC) through an acceleration of the colitis-dysplasia-carcinoma sequence of cellular transformation [5-7]. Although the probability of developing CAC appears to have declined, likely due to advancements in medical therapies and/or optimizations in endoscopic surveillance, CAC remains a dire consequence of long-standing UC [5, 8]. While frequent surveillance can reduce CAC incidence and mortality in patients with IBD [9], surveillance of IBD patient cohorts is challenged by concomitant inflammation, scarring, and flat dysplasia with indistinct margins [10]. The burden of colonoscopy surveillance may be eased with the discovery of biomarkers that can be routinely used to identify patients at high risk of developing dysplasia or CAC.

Mutational signature analysis of tissue and blood samples from CAC patients showed that the evolutionary trajectory of disease is initiated early in the colitis-dysplasia-carcinoma sequence [11]. Furthermore, the extent of colitis has been recognized as an independent and most significant risk factor for CAC [12]. In support of this, Bjerrum and colleagues provided transcriptional profiles of colonic mucosa from patients with varying extent of UC [13]. A gene expression dataset (GSE47908) was generated from mucosal biopsies sampled from the left colon of patients with left-sided colitis, pancolitis, or colitis-associated dysplasia (CAD) plus healthy controls. The authors identified differential transcriptional profiles aligned with UC extent (i.e., areas of involvement) that were not inferred by potential covariates in the clinical data (i.e., age, years with disease, Mayo score, and medication). Their findings suggest that gene expression profiles of colitis-associated lesions obtained from patients with varied extent of UC can be mined to support the development of molecular panels that identify patients at high risk of developing CAD or CAC [13]. However, additional network analyses and detailed mechanistic interrogation of specific molecular participants were not completed.

Elucidation of the mechanisms of colon carcinogenesis requires further investigation, and insight into the molecular events underpinning the progression of UC to colitis-associated colon cancer may be gained from the study of non-dysplastic colonic mucosa [11, 13]. The transcriptional dataset generated by Bjerrum and colleagues [13] provides an excellent resource to perform such an analysis. In this study, we performed differential expression analysis, pathway and network analyses, as well as differential correlation analysis on the GSE47908 dataset to determine how the extent of colitis impacts upon biological functions and regulatory pathways and to identify the key molecular factors that bridge the colitis-dysplasia progression. The results provide insight into the molecular events associated with colitis-dysplasia progression, which could be exploited for

the development of biomarkers in non-dysplastic mucosa that identify the risk of dysplasia for UC patients.

2. MATERIALS and METHODS

2.1. Data Processing - Data processing was completed using the R (v4.0.2) programming language, and all codes used in this study align with recommendations made by authors of R packages in their respective user's guide, which can be accessed at https://bioconductor.org.

2.2. Differential Gene Expression Analysis - Log transformed microarray expression data for GSE47908 and microarray platform data for GPL570 (HG-U133_Plus_2; Affymetrix Human Genome U133 Plus 2.0 Array) were retrieved from the GEO database available at https://www.ncbi.nlm.nih.gov/geo/ with the R package GEOquery. The limma R workflow [15] was used to detect differentially expressed transcripts between the UC clinical subtypes [left-sided colitis (n=20), pancolitis (n=19), colitis-associated dysplasia, CAD (n=6)], and healthy control (HC) samples (n=15). Specifically, the function |lmFit| was used to generate a linear model fit to the data matrix containing log expression values for GSE47908. Next, function |contrasts.fit| was used to compute estimated coefficients and standard error for a given set of contrasts (e.g., pancolitis vs. HC). Finally, function |eBayes| was used to compute log-odds of differential expression by empirical Bayes moderation of the standard errors towards a global value. All functions were operated with default settings.

Log-fold changes calculated by function |eBayes| for 54,675 transcripts, along with their false discovery ratio (FDR) and p-values, were uploaded to the Ingenuity Pathway Analysis (IPA) software. Some Affymetrix transcript identifiers remain unmapped by IPA; these genes were eliminated from the study, leaving 45,480 transcripts to be mapped. Due to redundancy of the

GeneChip HG-U133 Plus 2.0 Array, this transcript pool included duplicate genes. To resolve duplicates, IPA Core Analyses were performed on the mapped transcripts, and transcript identifiers were consolidated using their log_2FC measurement, by which, representative transcript was selected based on maximum absolute log_2FC. This returned 21,475 'analysis-ready' genes. To distinguish the differentially expressed genes (DEGs), the combined application of a stringent FDR threshold ($q < 0.001$) and a moderate fold change threshold ($|log_2FC| > 0.75$) was used. This reduced the number of false positives while maintaining the 'ideal' dataset size (200-3,000 genes) for subsequent IPA Core Analysis of gene expression data. Differential expression was then visualized via the EnhancedVolcano R package.

2.3. Functional Analysis of DEGs in UC disease subtypes - To compare DEGs and illustrate possible relationships between left-sided colitis, pancolitis, and CAD, a Venn diagram was first used to visualize the overlap of DEGs found in the three UC clinical subtypes. The lists of overlapping DEGs derived from the comparison of UC subtypes were then used as input data for gene ontology (GO) enrichment analysis, performed with the topGO R package. topGO was chosen owing to its *'elim'* method that takes GO hierarchy into consideration when calculating enrichment. For the enrichment analysis, the background consisted of all genes assessed by the microarray platform GPL570, and annotation was completed with the R package org.Hs.eg.db; GO terms with <10 annotations were excluded for interpretability. The degree of enrichment was reported as the odds ratio (OR), where I^A = # DEGs annotated with the GO term, I^B = # background genes annotated with the GO term, and OR = (I^A/size of DEG list) / (I^B/size of background list). Statistical significance was defined with a Fisher's Exact Test.

2.4. Ingenuity Pathway Analyses - To analyze changes in biological states across the UC clinical subtypes, three sets of IPA Core Analyses were performed, followed by IPA Comparison Analysis.

The IPA Comparison Analysis allows for side-by-side comparison of multiple Core Analyses, which facilitated the discovery of trends amongst the three datasets. Core Analyses were performed on the three datasets (i.e., left-sided colitis vs. HC, pancolitis vs. HC, and CAD vs. HC) to assess the canonical pathways, upstream regulators, molecular and cellular functions, and molecular interaction networks that were most likely to be perturbed based on the changes in gene expression. Within IPA, canonical pathways were built with reference to literature prior to DEG input and did not undergo structural changes upon DEG input. Instead, IPA computes a z-score that assesses the directionality within a gene set (i.e., the DEG input) to infer the activation state of each canonical pathway or molecular and cellular function. Upstream regulators were identified by the observed differential regulation of known downstream effector(s). The z-score determines the activation state of an upstream regulator by the regulation direction associated with the relationship from the upstream regulator to the effector(s). A negative z-score indicates inhibition, and a positive z-score indicates activation. Significance was calculated with the right-tailed Fisher's Exact Test. Changes in activation state across UC subtypes were assessed with Comparison Analysis (sort method = trend + z-score). The correlation of activation state as the extent of disease progressed from left-sided colitis to pancolitis to CAD (the trend) was examined, and the findings were reported as trending towards activation or trending towards deactivation.

2.5. Mapping Molecular Interaction Networks - DEGs from the three datasets were mapped to their corresponding gene objects in the Ingenuity Knowledge Base (IKB), and those that interacted with other molecules in the IKB were designated focus molecules. Focus molecules were then assembled into networks by maximizing their interconnectedness with each other (relative to non-focus molecules with which they are connected to in the IKB). While non-focus molecules from the IKB may be used to merge smaller networks into a larger network, networks are scored based

on the number of focus molecules they contain. Network size, the total number of focus molecules analyzed, and the total number of molecules in the IKB that could be included in the networks also contribute to the network scores. The score is a test of significance using hypergeometric distribution and is calculated with the right-tailed Fisher's Exact Test (Score = -log (Fisher's p-value; score ≥ 2 equals $p \leq 0.01$). For this study, networks were limited to 70 molecules each, and a maximum of 25 networks per UC-subtype were constructed. Individual networks (child networks, count = 75) were overlapped with one another to create a single parent network by virtue of common network molecules between child pairings; this was done with the RVenn R package. Finally, the edge betweenness parameter for the core network was computed via the NetworkAnalyzer app, included in Cytoscape v3.8.0.

2.6. Differential Correlations - A ggplot2-based R package, ggpubr (https://rpkgs.datanovia.com/ggpubr/), was used to investigate the relationship between the expression profiles of two genes. A Shapiro-Wilk normality test was conducted to refine probe-set redundancies for *YAP* and *DAPK3* probe-sets prior to completing the parametric correlation analyses (**Supplemental Figure S1**). Specifically, function |stat_cor| was used to calculate the Pearson correlation coefficient. The size of the concentration ellipse in normal probability was left at the default 0.95, which translates to a 95% confidence interval.

3. RESULTS

3.1. Analysis of Genes Differentially Expressed in UC Disease Subtypes.

The distribution of gene expression ratios (log-transformed) calculated between UC subtypes and healthy controls (HC) is presented in **Figure 1A**. For the left-sided colitis vs. HC comparison, 1,016 genes had $\log_2$FC greater than 0.75 ($q < 0.001$); of these DEGs, 614 were

upregulated, and 402 were downregulated. Pancolitis returned 2,858 DEGs, half of which were upregulated. Colitis-associated dysplasia (CAD) returned 1,842 DEGs; 393 were upregulated, and 1,449 were downregulated.

For functional predictions, a Venn diagram was first used to identify genes with expression regulation observed in multiple UC disease subtypes (**Supplemental Table A1**). As presented in **Figure 1B**, pancolitis overlapped both left-sided colitis and CAD in terms of common DEGs. Of the 2,858 pancolitis DEGs, 651 shared similar expression regulation as left-sided colitis DEGs (465 common upregulation plus 159 common downregulation), and 1,194 shared similar expression regulations as CAD DEGs (209 common upregulation plus 985 common downregulation). This feature was not observed when comparing left-sided colitis and CAD; less than 2% of the input DEGs appeared at the intersection of left-sided colitis ∩ pancolitis ∩ CAD. This analysis suggests pancolitis exists as the middle ground of UC subtypes that bridges the progression of UC from left-sided colitis to CAD. Thus, the DEGs located at the intersection of pancolitis ∩ left-sided colitis or pancolitis ∩ CAD were selected for functional analysis.

To identify the potential biological processes associated with UC clinical progression, two sets of DEGs at the intersection of 1) pancolitis ∩ left-sided colitis, or 2) pancolitis ∩ CAD were processed separately with the topGO R package for functional enrichment analysis. These enrichment analyses included both up-regulated and down-regulated genes. The top 10 terms from the 'Biological Process' (BP) category of the GO enrichment analysis are presented in **Figure 2**. The DEGs at the intersection of pancolitis and left-sided colitis were enriched in inflammatory processes (**Supplemental Table A2**) while the pancolitis ∩ CAD overlapping DEGs were enriched in actin-based processes (**Supplemental Table A3**). Specifically, the pancolitis ∩ left-sided colitis DEGs showed significant enrichment for the regulation of IFN-γ mediated signaling

pathways (GO:0060334), the antimicrobial humoral immune response mediated by antimicrobial peptide (GO:0061844), and the acute-phase response (GO:0006953) with 8.6-, 6.4-, and 6.0-fold enrichments, respectively. Across the pancolitis ∩ CAD DEGs, microvillus assembly (GO:0030033), Golgi to plasma membrane transport (GO:0006893), and actin cytoskeleton reorganization (GO:0031532) were found significantly over-represented with 6.3-, 3.1-, and 3.0-fold enrichments, respectively. Overall, the GO enrichment analysis suggests that as UC progressed from left-sided colitis to pancolitis to CAD, the transcriptome pattern also shifted from being immune-centric to having cytoskeleton-dependence. Presumably, the regulation of actin cytoskeleton organization plays an important role in colitis-dysplasia progression.

3.2. Association of Hippo Signaling Activation with Colitis-Dysplasia Progression.

To identify canonical pathways that are most relevant to the observed shift in gene expression profile, a comparison analysis heat map for canonical pathways significantly altered by UC disease subtypes was constructed (**Figure 3A**). This heatmap displays the trend of either activation or deactivation as the gene expression profile shifted in response to UC extent, that is, from left-sided colitis to pancolitis to CAD. The heatmap revealed Hippo signaling and Ephrin receptor signaling as the top canonical pathways that were progressively altered in concert with the pathogenic progression of UC. The Hippo signaling pathway displayed incremental activation, while the Ephrin receptor signaling pathway exhibited gradual deactivation as the UC extent broadened (**Figure 3A**). Diagrammatic comparison of Hippo and Ephrin receptor analyses conducted on UC-subtype DEGs are provided in **Supplemental Figure S2 and S3**, respectively.

Trends of activation or deactivation were also probed on upstream regulators and biological functions to obtain a basic view of the molecular mechanisms underlying the extent of colitis

(**Figure 3B**). In terms of upstream regulators, IL10RA exhibited a trend of increased activity whereas interferon (IFN)-γ exhibited a trend of decreased activity. Affected biological functions include apoptosis and cell movement, that underwent gradual activation and deactivation, respectively, as disease extended from left-sided colitis to pancolitis to CAD.

3.3. Actin Reorganization as a Potential Key Determinant for Colitis Progression.

Using the limma R-derived DEGs, the IPA software generated 25 networks for each of the three UC subtypes. Molecular network intersections, assembled with the RVenn R package, revealed a single parent network that connected all 75 child networks via 757 intersections/edges (**Figure 4A**). Among the 75 child networks, approximately two-third (48/75) were composed of less than 60 focus molecules (<85% focus molecules). The 757 intersections/edges that connected the child networks each comprise one to 24 common molecule overlaps. Nevertheless, over half (57%) of the interactions/edges were enabled by just one common molecule, and 87% of the edges involved less than four common molecules (<5% overlap). To reduce noise from the parent network depicted in **Figure 4A**, molecular network intersection was compiled once more, but with child networks that were built upon 60 or more focus molecules (>85% focus molecules) and preserving connections that were maintained by four or more common molecules (>5% overlap). This produced one core network of networks that connected 21 child networks with 21 edges; One intersection segment, though strongly connecting pancolitis network 6 to CAD network 10 with 24 common molecules (34% overlap), stood apart from the core network of networks (**Figure 4B**), so was excluded from subsequent analysis.

To pinpoint a network pairing that could be used to discern pathways or molecular processes bridging pancolitis to CAD, the ‘count of overlapping molecules’ and ‘value of edge betweenness’

measures were utilized for edge evaluation. Edge betweenness reflects the amount of control that an edge exerts over the interactions of other child networks in the parent network. The edge betweenness of e=(v,w) is defined as the number of shortest paths between two nodes that go through e divided by the total number of shortest paths that go from the two nodes [16, 17]. Edge betweenness does not consider the number of overlapping molecules that contribute to the intrinsic strength of each edge. Thus, additional consideration for this attribute was completed *post hoc*. As shown in **Figure 4B**, the edge connecting pancolitis network 15 to CAD network 1 stood out from the remaining network associations by virtue of its large number of overlapping molecules (20% overlap) and high value of edge betweenness (**Supplemental Table A4**). Taken together, the findings suggest that the removal of this edge may affect interactions between the remaining networks within network. Thus, the overlap between pancolitis network 15 and CAD network 1 was selected for further detailed examination.

The intersection pancolitis 15 ∩ CAD 1 was formed by 14 gene products, which, when analyzed for GO term enrichment, was predominantly composed of actin-based processes (**Figure 5A**). Specifically, the DEGs at this intersection showed significant enrichment for the ruffle organization (GO:0031529), the regulation of actin filament polymerization (GO:0030833), and the myofibril assembly (GO:0030239) with 66-, 33-, and 33- fold enrichments, respectively. However, within the confines of the IKB, none of the 13 focus molecules were directly linked to UC (**Figure 5B**). All probable shortest paths by which the focus molecules were connected to UC required at least one IPA-derived intermediate node. For the majority of indirect connections, gene products CTNNB1 (β-catenin), CDH1 (E-Cadherin), and TNF (Tumor Necrosis Factor) functioned as the IPA-derived intermediates.

3.4. Implication of DAPK3 as a Key Factor in the Colitis-Dysplasia Progression.

Further dissection of pancolitis 15 and CAD 1 revealed two signal transduction gene products that reside in the overlap of these two networks (**Table 1**). Namely, death-associated protein kinase 3 (DAPK3) as the sole protein kinase, and protein phosphatase PP1β catalytic subunit (PPP1CB) as the sole protein phosphatase. The remaining 12 gene products were categorized as either mechanochemical enzymes (i.e., motors) or scaffolding proteins involving the cytoskeleton. Both DAPK3 and PPP1CB were downregulated in pancolitis (log_2FC: -1.08, DAPK3; -1.56, PPP1CB) and CAD (log_2FC: -0.98, DAPK3; -1.52, PPP1CB) but showed no deregulation in left-sided colitis. Presumably, DAPK3 and PPP1CB act as key factors regulating the altered molecular pathways that bridge pancolitis to CAD.

3.5. Differential Correlation of DAPK3-YAP with UC Disease Progression.

Given the association of Hippo signaling activation with UC extent (**Figure 3A**), and the implication of *DAPK3* and *PPP1CB* as key factors in colitis-dysplasia progression (**Figure 5**), differential correlation analyses for the pairings *DAPK3-YAP* and *PPP1CB-YAP* were conducted to assess potential differences in gene-gene regulatory relationships among the UC disease subtypes. The GSE47908 dataset was generated using three probe sets for *DAPK3* (**Supplemental Figure S1A**), three probe sets for *YAP* (**Supplemental Figure S1B**) and four probe sets for *PPP1CB* (**Supplemental Figure S1C**). Resolution of probe set redundancy with the IPA software returned one representative probe set each for *DAPK3* (203890_s_at) and *PPP1CB* (228222_at); however, two representative probe sets (213342_at and 224894_at) were resolved for *YAP*. To identify the *YAP* probe set that best satisfied the assumption of a Pearson correlation, namely, that the expression values represented by the probe sets are normally distributed, the Shapiro-Wilk test

was performed separately for each probe set. Expression values represented by two of the three *YAP* probe sets (213342_at and 224894_at) conformed to a normal distribution (i.e., $p>0.05$ across all conditions). Additionally, expression values represented by probe set 2133342_at returned higher mean W-value (0.948 vs. 0.940 for 213342_at and 224894_at, respectively). As such, expression values represented by probe set 213342_at was utilized for subsequent Pearson correlation analysis. The Shapiro-Wilk test was also performed for the *DAPK3* and *PPP1CB* probe sets. While the representative *DAPK3* probe set selected by IPA (203890_s_at) passed the test of normality (**Supplemental Figure S1A**), the representative probe set selected by IPA for *PPP1CB* (228222_at) did not (i.e., with $p<0.05$ for left-sided colitis, the null hypothesis of normality was rejected; **Supplemental Figure S1C**). Because the *PPP1CB* expression values did not display a normal distribution, the Pearson's correlation test could not be used for population inferences. However, a relationship between the expression of *PPP1CB* and *YAP* for this sample set could still be inferred. As such, for the sake of continuity, expression values derived from probe set 228222_at were used to study whether there was some association between the expression of *PPP1CB* and *YAP* and to estimate the strength of this relationship.

As shown in **Figure 6A**, the *DAPK3-YAP* correlation in healthy controls was negative but flipped to positive in left-sided colitis. Moreover, as the UC disease extent progressed from left-sided colitis to pancolitis and then on to CAD, the *DAPK3-YAP* correlation grew progressively more positive. The general direction of differential correlation for the *PPP1CB-YAP* pairing mirrors that of the *DAPK3-YAP* pairing (**Figure 6B**). However, the differential correlation with UC disease extent was less apparent for the *PPP1CB-YAP* pairing. This result suggests that changes in the potential regulatory relationship between DAPK3 and YAP, conditioned on UC disease extent, may contribute to disease progression.

4. DISCUSSION

In UC, prolonged disease duration and extensive intestinal involvement (i.e., pancolitis) are associated with an increased risk for colorectal cancer [12]. The progression of carcinogenesis in UC is thought to be driven by chronic inflammation and proceeds in a stepwise manner through a colitis-dysplasia-carcinoma sequence [5, 6]. As the area affected by UC grows so too does the inflammatory load which could in turn accelerate dysplasia and CAC tumorigenesis [18]. While the impact that inflammation can have on colon carcinogenesis should not be discounted, evidence also suggests that non-inflammatory factors play a role in mediating the colitis-dysplasia-carcinoma progression [7, 18, 19]. Among patients or animals with similar inflammatory status, some develop CAC while others do not [7]. Additionally, whole-exome sequence analysis of IBD-associated colorectal cancer showed that, apart from rare cases of mutations in DNA proofreading or repair pathways, supra-IBD inflammation alone does not compel greater mutation rates when compared with sporadic CRC of non-inflammatory origin [19]. This also supports a role for non-inflammatory factors in mediating colitis-dysplasia-carcinoma progression. As an example, azoxymethane (AOM)-treated *IL10*-/- mice infected with colitogenic *E. coli* NC101 or *E. faecalis* OG1RF exhibited a similar degree of colitis and comparable levels of immune infiltrate; tumors were only observed in 10% of *E. faecalis*-infected mice whereas 80% of *E. coli*-infected mice showed tumor development. The polyketide synthase (*pks*) genotoxic island, found in *E. coli* NC101 but not *E. faecalis* OG1RF, was linked to the DNA damage and subsequent tumorigenesis in the *E. coli* infected mice [20]. Moreover, gene mutation and gene expression analyses have linked cytoskeleton remodeling to colitis-dysplasia-carcinoma progression [19, 21, 22]. Our investigation verified pancolitis as a conduit for UC advancement from left-sided colitis to CAD and confirmed

dysregulation of actin reorganization as a key determinant for the progression of UC from non-dysplastic to dysplastic UC.

Bjerrum *et al*. previously defined distinct gene expression signatures for dysplasia versus pancolitis, dysplasia versus left-sided UC, and pancolitis versus left-sided UC in the GSE47908 dataset [13]. These expression signatures manifested GO terms for left-sided UC (i.e., *protein metabolic process* and *cell cycle process*) that distinguished the early disease stage from pancolitis and dysplasia (i.e., *protein export from nucleus* and *response to insulin stimulus*). Our output of GO enrichment terms identifies the dysregulation of inflammatory processes to exist at the intersection of pancolitis and left-sided UC. These terms would be excluded from the original Bjerrum analysis since statistical filtering was employed to eliminate DEGs that were solely reflective of inflammation. In addition, our inquiry also uniquely revealed that the intersection of pancolitis with CAD was rooted in the dysregulation of actin-based processes (i.e., *actin cytoskeleton reorganization* and *microvillus assembly*). Bjerrum *et al*. further extracted a panel of transcripts for therapeutic importance based on their known involvement in inflammatory and neoplastic processes; MAPK-interacting serine/threonine protein kinase 2 (*MKNK2*) and insulin receptor alpha (*INSRA*) were authenticated as potential critical transcripts for inflammation-driven tumorigenesis. Laminin γ2 (*LAMC2*) was also highlighted as a biomarker of preneoplastic lesions in UC that still awaits validation. In our analyses, these DEGs also exist solely within specific disease types (**Supplemental Table A1**); their absence from the DEG networks that bridge between pancolitis and CAD suggest that distinct signaling mechanisms are responsible for the progression and the maintenance of disease states.

Subsequent to the Bjerrum *et al*. study, the GSE47908 dataset was also used by investigators to interrogate key genes and/or biological processes in the context of UC progression. Most

commonly, GSE47908 was combined with other datasets from the Gene Expression Omnibus (GEO) to conduct differential expression comparison of UC versus normal samples. As an example, Kaiko and colleagues included GSE47908 as part of their multi-institute retrospective cohort study which identified plasminogen activator inhibitor-1 as a link between the epithelium and inflammation [14]. Unfortunately, when these studies consolidated GSE47908 with other GEO datasets, the key strength of GSE47908 was inadvertently lost. That is, the extent of disease, which may affect transcriptional profiles, was no longer accounted for.

The prominent positioning of actin-based processes within the network intersection of pancolitis and CAD (**Figure 5**) substantiates results of a gene expression analysis of patients with CAC presented by Kanaan and colleagues, that established actin cytoskeleton organization as the most significantly disrupted process in UC progression [21]. Protein abundance analysis of UC progressors (UC patients with CAD or CAC) versus non-progressors has also identified enrichment of dysregulated cytoskeletal proteins in UC progressors [23]. Drawbacks in these two studies include the evaluation of UC progression in a binary fashion (presence or absence of CAD and/or CAC) as well as the small sample sizes (i.e., three unique patients in the study conducted by Kanaan and colleagues [21], and 15 unique patients in the study conducted by May and colleagues [23]). To provide insight into the molecular events associated with the stepwise progression of UC, it will be necessary to demonstrate that the dysregulations observed in CAD or CAC were issued forth from some form of non-dysplastic UC.

Signal transduction pathways regulate many cellular functions that were found altered in UC carcinogenesis, such as proliferation, growth, differentiation, metabolism, and survival. Molecular investigations have previously associated STAT3, Wnt, TGF-β, and TLR4/NFκB signaling with the pathogenesis of colon carcinogenesis [24-26]. However, the pathways most relevant to the gene

expression changes observed during the early progression of UC, before any histological evidence of dysplasia/carcinoma, remain unknown. In this regard, Hippo signaling and Ephrin receptor signaling were uncovered as the top canonical pathways that were progressively altered in concert with the extent of UC progression (**Figure 3A**). The Hippo pathway is a fundamental signaling cascade that negatively regulates the activity of YAP/TAZ to coordinate cell proliferation, apoptosis, and cell movement; as such, it is essential for tissue homeostasis, repair, and regeneration [27]. Importantly, YAP/TAZ-mediated cell proliferation in epithelial monolayers is controlled by a cytoskeletal checkpoint, which in turn, is monitored by actin-processing factors. The Ephrin pathway also controls intestinal homeostasis through cell proliferation and cell movement additionally to cell attachment and repulsion [28, 29]. However, deciphering functional outcomes by Ephrin pathway activation is circuitous due to the redundancy and idiosyncrasy of this pathway [30]. The Ephrin receptors (Eph) comprise the largest family of receptor tyrosine kinases (RTK). But, unlike most RTKs for which ligands are generally soluble, the cognate ligands of Eph receptors, the ephrins, are also membrane bound. This aspect of the Eph-ephrin receptor-ligand pairing consequently induces bidirectional signaling, where signaling through Eph is termed forward signaling and through ephrin is termed reverse signaling. Furthermore, there is a plethora of Ephs and ephrins (i.e., 14 Ephs, 8 ephrins) with promiscuous pairing options. Eph/ephrin also exhibits *cis* interactions to inhibit forwarding signaling. Ephrin is therefore a more convoluted pathway to render (**Supplemental Figure S3**), relative to the Hippo pathway (**Supplemental Figure S2**).

The Hippo pathway was previously identified as a key factor for the compensatory regeneration of IECs in response to tissue injury using a colitis mouse model [31]. The recent emergence of YAP as a potential regulator of intestinal diseases involves elements beyond the

canonical Hippo pathway. For one, YAP can be sequestered at adherens junctions (AJs) via interactions with α-catenin [32], the abundance of which is significantly altered in active UC [33]. Secondly, nuclear translocation of YAP may be brought about via stimulation of gp130-associated Src family kinase Yes [34]. Finally, YAP was found to be a crucial pivot point of cellular reprograming during intestinal epithelial repair, coupling epithelial restitution to the proliferative phase of regeneration by way of FAK-Src signaling [35]. In view of YAP as a mechanosensor and mechanotranducer amidst epithelial regeneration of injured tissue, a comprehensive understanding of the interplay between YAP and the actin cytoskeleton is needed to make rational selections of therapeutic targets for patients at high risk of UC neoplastic progression.

The identification of DAPK3 as a potential key factor in UC progression is particularly interesting. DAPK3 was shown to influence the proliferation of colon cancer cells [36]; however, a role for DAPK3 in UC pathogenesis (i.e., within the context of colitis or colitis-associated dysplasia-carcinoma) was unknown prior to this study. DAPK1, the closely related family member and upstream regulator of DAPK3, was previously associated with UC severity [37] and gastrointestinal cancer pathogenesis [38]. In addition, pharmacological inhibition of DAPK1 was reported to augment susceptibility to DSS-induced colitis in mice, with concomitant increase in bacterial translocation ascribed to epithelial barrier defects [39]. It is regrettable that the small molecule inhibitor of DAPK1 (i.e., DAPK6) applied in the study of tunicamycin (TM)-induced, ER-stress-dependent reduction of bacterial translocation, potently cross-inhibits DAPK3 (IC_{50}=225 nM [40]) and Rho-associated coil-coiled kinase (ROCK, K_i=132 nM [41]). Although the Lopes study included siRNA knockdown experiments to independently validate DAPK1 signaling involvement, the potential impact of concurrent DAPK3 and ROCK inhibition brought forth with the DAPK6 inhibitor was not examined. Previously, Ito and colleagues showed that ROCK activity

increased in response to TM, and that treatment with Y27632 (a selective ROCK inhibitor) completely reversed TM-induced ER-stress responses in the J774 macrophage cell line [42]. Moreover, the involvement of DAPK3 in ER-stress response was also demonstrated in human aortic vascular smooth muscle cells, where shRNA-mediated silencing of *DAPK3* ablated the calcifying-media induced increase of CCAAT-enhancer-binding protein homologous protein (CHOP), a multifunctional transcription factor in ER-stress response [43]. In the same study, treatment with DAPK6 attenuated vascular calcification in rats, alongside a significant reduction in CHOP protein abundance in the aorta. It may be beneficial to learn whether DAPK3 and/or ROCK alter ER-stress-dependent autophagy in the context of DSS-induced colitis in mice.

Some limitations in the present study are apparent. First, the progression of UC to CAD occurs through multiple mechanisms involving various cell types. The analyses were completed on transcriptional profiles generated from mucosal biopsies, and genes may demonstrate diverse functions across different cell types. Hence, the gene sets identified from the averaged tissue dataset will require re-examination in a cell type-specific way (e.g., single cell RNA-Seq) to precisely identify the susceptible cell types and convergent pathways among different cells. Second, we were unable to identify additional publicly available datasets that specifically assessed gene expression in inflamed (involved) colon tissues of UC patients with adequate control for the relationship between colonic biopsy location and gene expression. Five data series (i.e., GSE37283 [44], GSE38713 [45], GSE48634 [46], GSE105074 [47], and GSE87466 [48]) were considered as potential verification and comparison cohorts since these possess gene expression data for colonic biopsies obtained from healthy controls and UC patients grouped by disease extension (i.e., left-sided colitis vs. pancolitis). Unfortunately, GSE48634, GSE105074 and GSE87466 were eliminated as appropriate verification datasets due to critical differences in the location and inflammatory status

of biopsies. In these cases, the biopsy location was associated with greater variation than disease extent (**Supplemental Figure S4**). However, *DAPK3* expression in the GSE38713 data series was significantly downregulated in left-sided colitis (log-FC=-1.42, FDR=0.006; remission involved biopsies) as well as in pancolitis (log-FC=-1.74, FDR=0.04; remission involved biopsies). Differential correlation analysis of *DAPK3-YAP* expression across the active involved groupings showed loss of relationship between *DAPK3* and *YAP* as disease transitioned from normal to left-sided active involved, and then to pancolitis active involved (**Supplemental Figure S5**). In addition, a negative correlation for *DAPK3-YAP* was corroborated in healthy controls of the GSE37283 dataset [44]. The relationship flipped to positive in UC patients harboring a remote neoplastic lesion (**Supplemental Figure S6**), confirming the *DAPK3-YAP* relationships identified in the Bjerrum data series (**Figure 6A**). Finally, the results of this study represent a data mining activity, so additional well-designed investigations will be required for validation of findings. Despite these drawbacks, independent confirmations and similarities among verification cohorts provide a high level of confidence in the overall significance of *DAPK3* and *YAP* in UC neoplastic progression.

5. CONCLUSION

The probability that DAPK3 plays a role in the progression of the pathological changes of UC is notable. To substantiate the connection of DAPK3 to UC progression, the difference in correlation between *DAPK3* and *YAP* was studied in all UC clinical subtypes plus healthy control samples. Differential co-expression operates on the level of gene pairs and is used as an alternative approach to identify disease-related genes [49]. Results from the differential co-expression analyses demonstrate the correspondence of *DAPK3-YAP* correlation with UC extent. This suggests that changes in the potential regulatory relationship between DAPK3 and YAP, conditioned on UC

extent, may contribute to UC progression. Still, the driver(s) behind the differential *DAPK3–YAP* co-expression pattern is unclear. Better understanding of the relationship between YAP and DAPK3 may enable the discovery of targeted therapy for the prevention of UC neoplastic progression.

6. ACKNOWLEDGEMENTS

This work was supported by a research grant from the Canadian Institutes of Health Research (MOP#97931 to J.A.M.). H.-M.C. was recipient of CIHR Fredrick Banting and Charles Best Canada and Alberta Graduate Excellence Scholarships.

7. AUTHOR CONTRIBUTIONS

H.-M.C. completed the data analysis, prepared figures and wrote the manuscript. J.A.M. conceived and coordinated the study, wrote the manuscript, supervised trainees and provided intellectual contributions to the project. All authors reviewed the results and approved the final version of the manuscript.

TABLE 1. Overlapping gene products in the pancolitis 15 ∩ CAD network 1 intersection.

Gene	Protein	Molecular Function	Expression FC		
			L	P	D
DAPK3	Death-associated protein kinase 3	Kinase	-0.15	-1.08§	-0.98§
PPP1CB	Protein phosphatase PP1β subunit	Phosphatase	-0.12	-1.56§	-1.52§
MYO1C	Unconventional myosin IC	Motor	-0.18	0.77*	0.99*
MYO6	Unconventional myosin VI	Motor	-0.31	-0.88§	-1.36§
ARHGAP21	Rho GTPase-activating protein 21	GTPase	-0.48	-0.98§	-0.97§
CAPZA1	F-actin-capping protein α1	Actin Binding	0.18	-1.89§	-2.21§
CORO1B	Coronin 1B	Actin Binding	-0.08	0.88*	0.86*
CPNE8	Copine 8	Membrane Binding	-0.34	-1.55§	-1.93§
DCTN5	Dynactin 5	Scaffold	-0.20	-0.80§	-1.64§
FLNB	Filamin B	Actin Binding	-0.49	-0.76§	-1.20§
FLOT2	Flotillin 2	Scaffold	0.17	-0.78§	-0.95§
TMOD3	Tropomodulin 3	Actin Binding	-0.22	-1.36§	-2.15§
TPM1	Tropomyosin α1	Actin Binding	-0.61	-0.86§	1.01*
---	Monomeric (G) actin	Structural	Not a focus molecule		

FC = $\log_2$ fold-change, L = left-sided colitis, P = pancolitis, and D = colitis-associated dysplasia. A gene was deemed dysregulated when $|\log_2 FC|>0.75$ and FDR<0.001; * - significant upregulation, § - significant downregulation.

FIGURE LEGENDS

Figure 1. Differential expression of genes in UC disease subtypes. (**A**), differential gene expression of three UC clinical subtypes against healthy controls. Log_2FC calculated with limma R for the GSE47908 dataset [n = 15 (healthy controls, HC), n = 20 (left-sided colitis), n = 19 (pancolitis), and n = 6 (colitis-associated dysplasia, CAD)]. The threshold set for log_2FC was |0.75|. Significance was determined by FDR<0.001. (**B**), overlap of shared differentially expressed genes (DEGs) between UC subtypes. The proportional Venn diagram was generated with Bio Venn and then optimized with eulerAPE_3.0.0.jar.

Figure 2. Gene ontology (GO) term enrichment analysis of differentially expressed genes (DEGs) common among UC subtypes. DEGs at the intersection of pancolitis ∩ left-sided colitis or pancolitis ∩ CAD were subjected to GO term enrichment analysis for Biological Process categories. Enrichment was performed with topGO R ("elim" algorithm, "fisher" statistic). Statistical significance was defined with a Fisher's Exact Test.

Figure 3. Ingenuity Pathway Analysis (IPA) of canonical pathways, upstream regulators and functions differentially deregulated among UC subtypes. For each colitis subtype, the activation z-score calculated by IPA software predicts the activation (red) or inhibition (blue) potential for each canonical pathway **(A)** or regulator/function **(B)**. The reports are sorted based on correlation of z-scores to extent of disease (left-sided colitis to pancolitis to CAD) with higher total scores across the colitis-subtypes ranked higher than those with lower total scores. LS: left-sided colitis, Pan: pancolitis, Dys: CAD.

Figure 4. Intersections of UC clinical subtype molecular interactions. Molecular networks were constructed for each UC subtype. Octagons represent networks constructed with CAD DEGs, hexagons represent pancolitis networks, and rectangles indicate left-sided colitis networks. Shape size represents the relative number of DEGs used to build each network. The networks are connected to each other if there are any overlapping gene products, and line width represent the number of shared gene products. The serpentine network overlap (**A**) was detangled by focusing on networks that had >85% of DEG inputs and keeping edges that involved >5% overlap of gene products. This returned a core network of networks (**B**) that was heavily leveraged on the edge connecting CAD network 1 and pancolitis network 15 (red).

Figure 5. Gene ontology (GO) term enrichment analysis of the pancolitis network 15 and CAD network 1 intersection. In (**A**), DEGs at the intersection of pancolitis network 15 ∩ CAD (colitis-associated dysplasia) network 1 were subjected to GO term enrichment analysis for Biological Process categories. Network was constructed by IPA software, and intersections compiled with RVenn R. Edge-betweenness was computed by the Cytoscape app NetworkAnalyzer. Enrichment performed with topGO R. Statistical significance was defined with a Fisher's Exact Test. In (**B**), the shortest paths linking the 13 focus molecules to the disease ulcerative colitis were established using the IPA Path Explorer tool. The 13 focus molecules (highlighted in yellow) were used as the starting point for the generation of biological networks based on their connectivity as established in the Ingenuity Knowledge Base (IKB). Incorporating findings from experimentally observed/highly predicted confidence levels and direct/indirect interactions, the IPA Path Explorer tool built 88 shortest paths to connect focus molecules through

a minimum of one IPA-derived intermediate molecule to the disease ulcerative colitis. All probable shortest paths by which the focus molecules were connected to the disease ulcerative colitis required at least one interconnecting gene product (i.e., none of the lines originating from any of the focus molecules (colored in light blue) connect directly to the disease ulcerative colitis).

Figure 6. Differential correlation of *DAPK3*-*YAP* and *PPP1CB*-*YAP* relationships. The main panels display the relationship between the log-transformed expression profiles of (**A**) *DAPK3* and *YAP* or (**B**) *PPP1CB* and *YAP*. These scatterplots are overlayed with confidence ellipses of covariance, constructed for the 95% CI. In the marginal box plots of log-transformed gene expression, the lower whisker represents the lowest datum still within 1.5 interquartile range (IQR) of the lower quartile, and the upper whisker represents the highest datum still within 1.5 IQR of the upper quartile.

REFERENCES

1 Ordas I, Eckmann L, Talamini M, Baumgart DC, Sandborn WJ. Ulcerative colitis. *Lancet*. 2012;380(9853):1606-1619.

2 Porter RJ, Kalla R, Ho GT. Ulcerative colitis: Recent advances in the understanding of disease pathogenesis. *F1000Res*. 2020;9.

3 Younis N, Zarif R, Mahfouz R. Inflammatory bowel disease: between genetics and microbiota. *Mol Biol Rep*. 2020;47(4):3053-3063.

4 Jostins L, Ripke S, Weersma RK, et al. Host-microbe interactions have shaped the genetic architecture of inflammatory bowel disease. *Nature*. 2012;491(7422):119-124.

5 Dulai PS, Sandborn WJ, Gupta S. Colorectal Cancer and Dysplasia in Inflammatory Bowel Disease: A Review of Disease Epidemiology, Pathophysiology, and Management. *Cancer Prev Res (Phila)*. 2016;9(12):887-894.

6 Low D, Mino-Kenudson M, Mizoguchi E. Recent advancement in understanding colitis-associated tumorigenesis. *Inflamm Bowel Dis*. 2014;20(11):2115-2123.

7 Van Der Kraak L, Gros P, Beauchemin N. Colitis-associated colon cancer: Is it in your genes? *World J Gastroenterol*. 2015;21(41):11688-11699.

8 Kabir M, Fofaria R, Arebi N, et al. Systematic review with meta-analysis: IBD-associated colonic dysplasia prognosis in the videoendoscopic era (1990 to present). *Aliment Pharmacol Ther*. 2020;52(1):5-19.

9 Ananthakrishnan AN, Cagan A, Cai T, et al. Colonoscopy is associated with a reduced risk for colon cancer and mortality in patients with inflammatory bowel diseases. *Clin Gastroenterol Hepatol*. 2015;13(2):322-329 e321.

10 Ullman T, Odze R, Farraye FA. Diagnosis and management of dysplasia in patients with ulcerative colitis and Crohn's disease of the colon. *Inflamm Bowel Dis*. 2009;15(4):630-638.

11 Baker AM, Cross W, Curtius K, et al. Evolutionary history of human colitis-associated colorectal cancer. *Gut*. 2019;68(6):985-995.

12 Zhou Q, Shen ZF, Wu BS, et al. Risk of Colorectal Cancer in Ulcerative Colitis Patients: A Systematic Review and Meta-Analysis. *Gastroenterol Res Pract*. 2019;2019:5363261.

13 Bjerrum JT, Nielsen OH, Riis LB, et al. Transcriptional analysis of left-sided colitis, pancolitis, and ulcerative colitis-associated dysplasia. *Inflamm Bowel Dis*. 2014;20(12):2340-2352.

14 Kaiko GE, Chen F, Lai CW, et al. PAI-1 augments mucosal damage in colitis. *Sci Transl Med*. 2019;11(482).

15 Ritchie ME, Phipson B, Wu D, et al. limma powers differential expression analyses for RNA-sequencing and microarray studies. *Nucleic Acids Res*. 2015;43(7):e47.

16 Newman ME, Girvan M. Finding and evaluating community structure in networks. *Phys Rev E Stat Nonlin Soft Matter Phys*. 2004;69(2 Pt 2):026113.

17 Yoon J, Blumer A, Lee K. An algorithm for modularity analysis of directed and weighted biological networks based on edge-betweenness centrality. *Bioinformatics*. 2006;22(24):3106-3108.

18 Grivennikov SI, Cominelli F. Colitis-Associated and Sporadic Colon Cancers: Different Diseases, Different Mutations? *Gastroenterology*. 2016;150(4):808-810.

19 Robles AI, Traverso G, Zhang M, et al. Whole-Exome Sequencing Analyses of Inflammatory Bowel Disease-Associated Colorectal Cancers. *Gastroenterology*. 2016;150(4):931-943.
20 Arthur JC, Perez-Chanona E, Muhlbauer M, et al. Intestinal inflammation targets cancer-inducing activity of the microbiota. *Science*. 2012;338(6103):120-123.
21 Kanaan Z, Qadan M, Eichenberger MR, Galandiuk S. The actin-cytoskeleton pathway and its potential role in inflammatory bowel disease-associated human colorectal cancer. *Genet Test Mol Biomarkers*. 2010;14(3):347-353.
22 Majumdar D, Tiernan JP, Lobo AJ, Evans CA, Corfe BM. Keratins in colorectal epithelial function and disease. *Int J Exp Pathol*. 2012;93(5):305-318.
23 May D, Pan S, Crispin DA, et al. Investigating neoplastic progression of ulcerative colitis with label-free comparative proteomics. *J Proteome Res*. 2011;10(1):200-209.
24 Claessen MM, Schipper ME, Oldenburg B, Siersema PD, Offerhaus GJ, Vleggaar FP. WNT-pathway activation in IBD-associated colorectal carcinogenesis: potential biomarkers for colonic surveillance. *Cell Oncol*. 2010;32(4):303-310.
25 Muller M, Hansmannel F, Arnone D, et al. Genomic and molecular alterations in human inflammatory bowel disease-associated colorectal cancer. *United European Gastroenterol J*. 2020;8(6):675-684.
26 Tang A, Li N, Li X, et al. Dynamic activation of the key pathways: linking colitis to colorectal cancer in a mouse model. *Carcinogenesis*. 2012;33(7):1375-1383.
27 Park J, Hansen CG. Cellular feedback dynamics and multilevel regulation driven by the hippo pathway. *Biochem Soc Trans*. 2021;49(4):1515-1527.
28 Grandi A, Zini I, Palese S, et al. Targeting the Eph/Ephrin System as Anti-Inflammatory Strategy in IBD. *Front Pharmacol*. 2019;10:691.
29 Perez White BE, Getsios S. Eph receptor and ephrin function in breast, gut, and skin epithelia. *Cell Adh Migr*. 2014;8(4):327-338.
30 Arvanitis D, Davy A. Eph/ephrin signaling: networks. *Genes Dev*. 2008;22(4):416-429.
31 Cai J, Zhang N, Zheng Y, de Wilde RF, Maitra A, Pan D. The Hippo signaling pathway restricts the oncogenic potential of an intestinal regeneration program. *Genes Dev*. 2010;24(21):2383-2388.
32 Schlegelmilch K, Mohseni M, Kirak O, et al. Yap1 acts downstream of alpha-catenin to control epidermal proliferation. *Cell*. 2011;144(5):782-795.
33 Karayiannakis AJ, Syrigos KN, Efstathiou J, et al. Expression of catenins and E-cadherin during epithelial restitution in inflammatory bowel disease. *J Pathol*. 1998;185(4):413-418.
34 Taniguchi K, Wu LW, Grivennikov SI, et al. A gp130-Src-YAP module links inflammation to epithelial regeneration. *Nature*. 2015;519(7541):57-62.
35 Yui S, Azzolin L, Maimets M, et al. YAP/TAZ-Dependent Reprogramming of Colonic Epithelium Links ECM Remodeling to Tissue Regeneration. *Cell Stem Cell*. 2018;22(1):35-49 e37.
36 Togi S, Ikeda O, Kamitani S, et al. Zipper-interacting protein kinase (ZIPK) modulates canonical Wnt/beta-catenin signaling through interaction with Nemo-like kinase and T-cell factor 4 (NLK/TCF4). *J Biol Chem*. 2011;286(21):19170-19177.

37 Kuester D, Guenther T, Biesold S, et al. Aberrant methylation of DAPK in long-standing ulcerative colitis and ulcerative colitis-associated carcinoma. *Pathol Res Pract*. 2010;206(9):616-624.
38 Yuan W, Chen J, Shu Y, et al. Correlation of DAPK1 methylation and the risk of gastrointestinal cancer: A systematic review and meta-analysis. *PLoS One*. 2017;12(9):e0184959.
39 Lopes F, Keita AV, Saxena A, et al. ER-stress mobilization of death-associated protein kinase-1-dependent xenophagy counteracts mitochondria stress-induced epithelial barrier dysfunction. *J Biol Chem*. 2018;293(9):3073-3087.
40 Okamoto M, Takayama K, Shimizu T, Ishida K, Takahashi O, Furuya T. Identification of death-associated protein kinases inhibitors using structure-based virtual screening. *J Med Chem*. 2009;52(22):7323-7327.
41 Al-Ghabkari A, Deng JT, McDonald PC, et al. A novel inhibitory effect of oxazol-5-one compounds on ROCKII signaling in human coronary artery vascular smooth muscle cells. *Sci Rep*. 2016;6:32118.
42 Ito H, Yamashita Y, Tanaka T, et al. Cigarette smoke induces endoplasmic reticulum stress and suppresses efferocytosis through the activation of RhoA. *Sci Rep*. 2020;10(1):12620.
43 Li KX, Du Q, Wang HP, Sun HJ. Death-associated protein kinase 3 deficiency alleviates vascular calcification via AMPK-mediated inhibition of endoplasmic reticulum stress. *Eur J Pharmacol*. 2019;852:90-98.
44 Pekow J, Dougherty U, Huang Y, et al. Gene signature distinguishes patients with chronic ulcerative colitis harboring remote neoplastic lesions. *Inflamm Bowel Dis*. 2013;19(3):461-470.
45 Planell N, Lozano JJ, Mora-Buch R, et al. Transcriptional analysis of the intestinal mucosa of patients with ulcerative colitis in remission reveals lasting epithelial cell alterations. *Gut*. 2013;62(7):967-976.
46 Smith PJ, Levine AP, Dunne J, et al. Mucosal transcriptomics implicates under expression of BRINP3 in the pathogenesis of ulcerative colitis. *Inflamm Bowel Dis*. 2014;20(10):1802-1812.
47 Vinayaga-Pavan M, Frampton M, Pontikos N, et al. Elevation in Cell Cycle and Protein Metabolism Gene Transcription in Inactive Colonic Tissue From Icelandic Patients With Ulcerative Colitis. *Inflamm Bowel Dis*. 2019;25(2):317-327.
48 Li K, Strauss R, Ouahed J, et al. Molecular Comparison of Adult and Pediatric Ulcerative Colitis Indicates Broad Similarity of Molecular Pathways in Disease Tissue. *J Pediatr Gastroenterol Nutr*. 2018;67(1):45-52.
49 McKenzie AT, Katsyv I, Song WM, Wang M, Zhang B. DGCA: A comprehensive R package for Differential Gene Correlation Analysis. *BMC Syst Biol*. 2016;10(1):106.

Figure 1

A

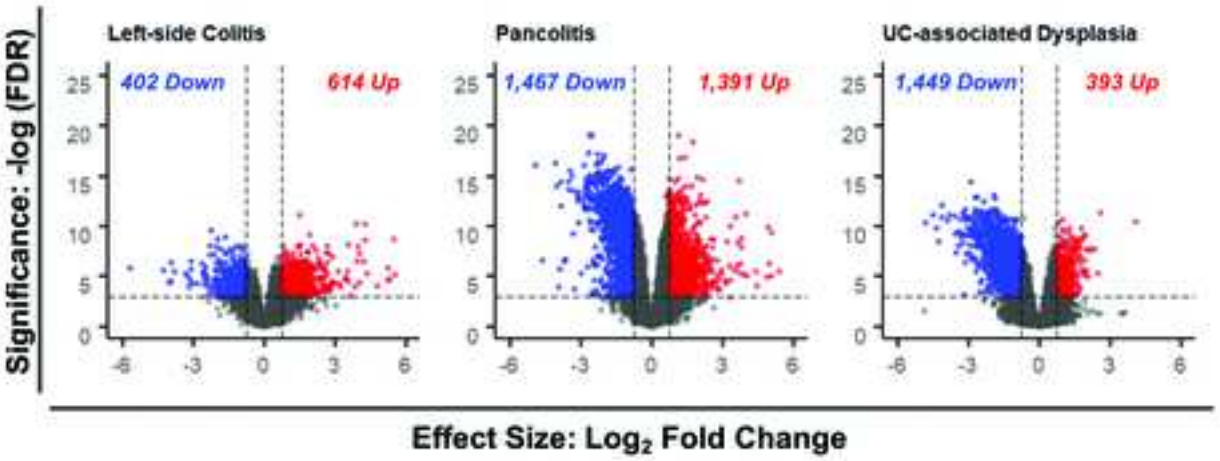

B

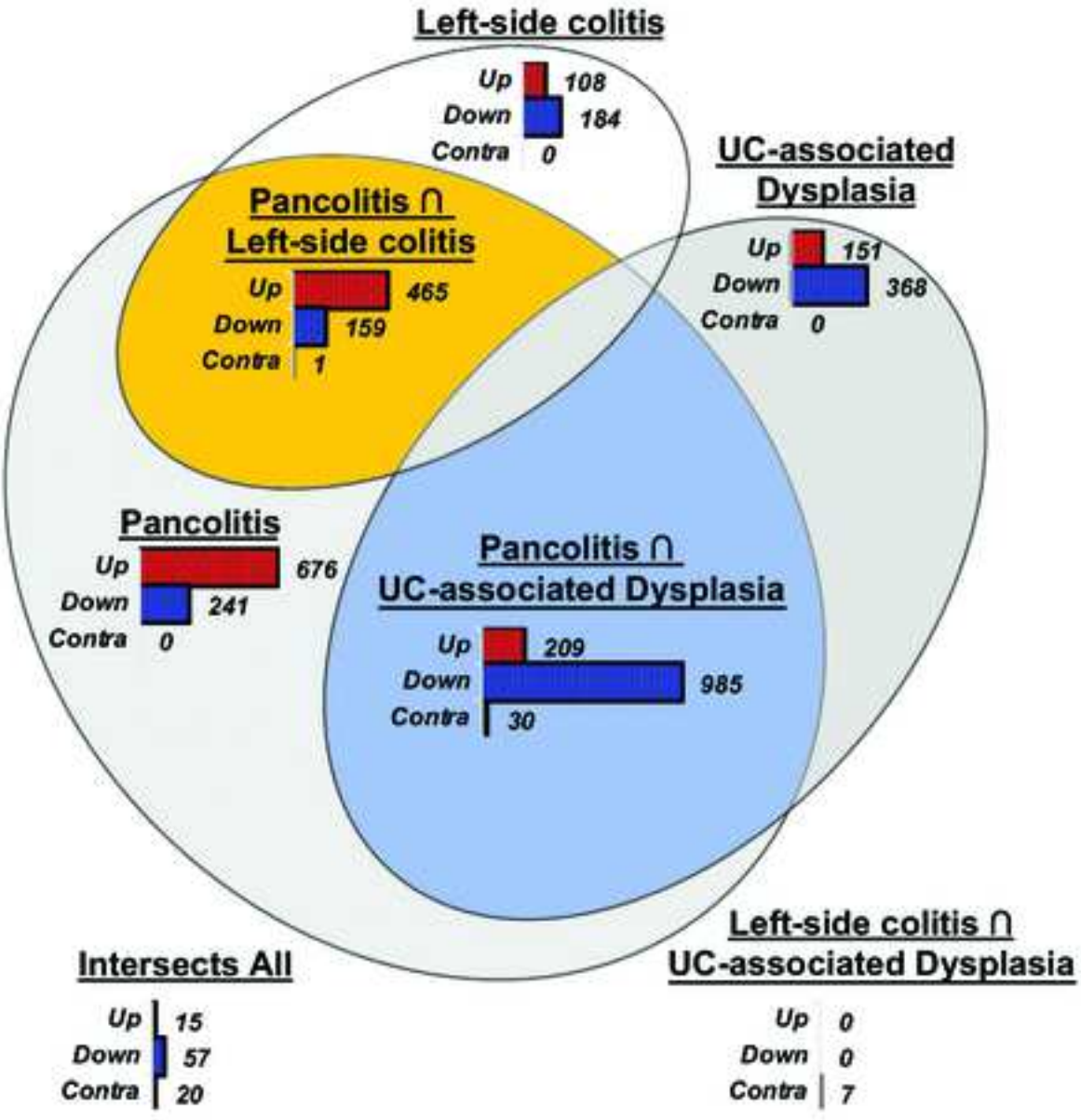

Figure 2

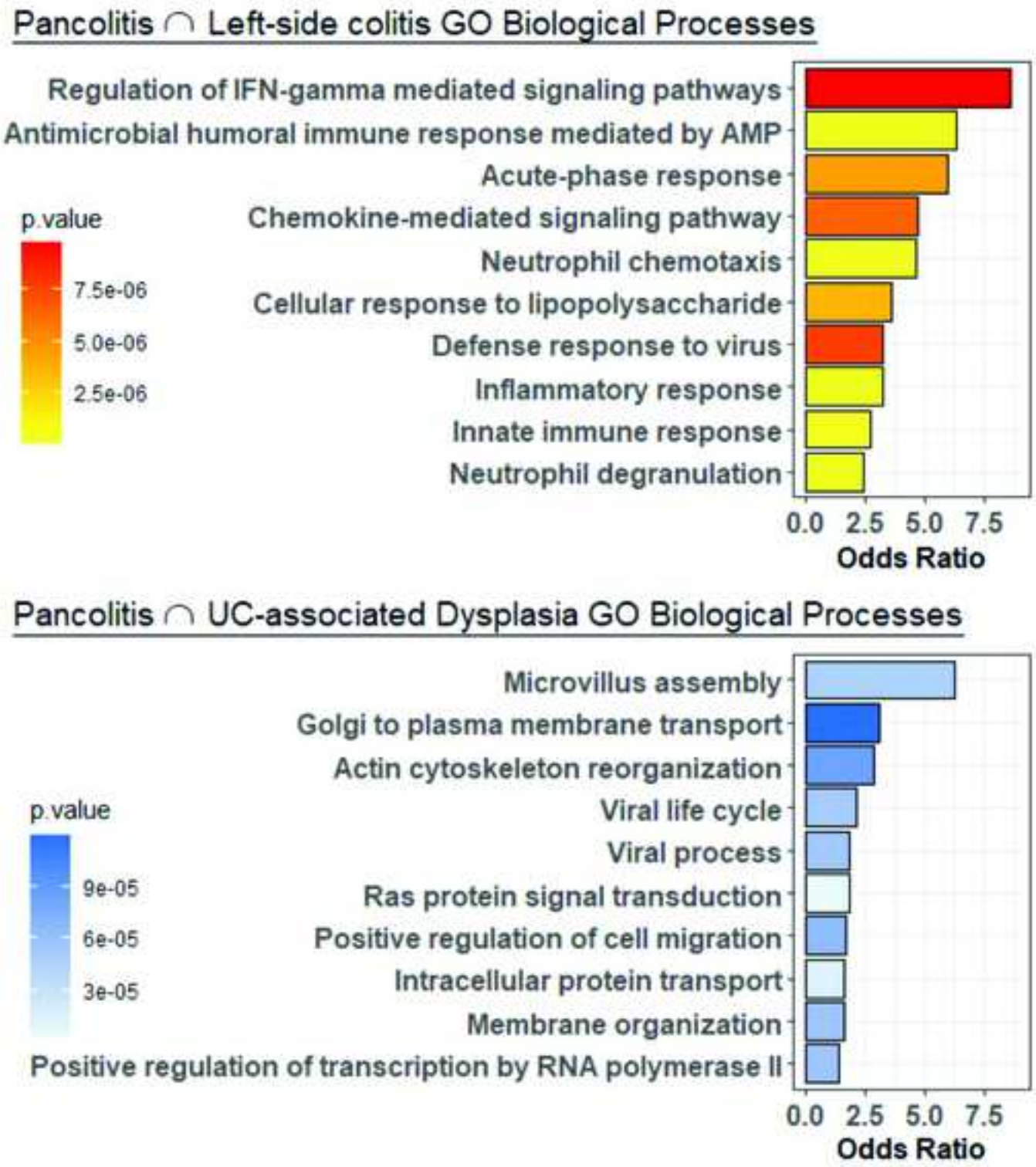

Figure 3

Click here to access/download;Image;Figure 3.tif

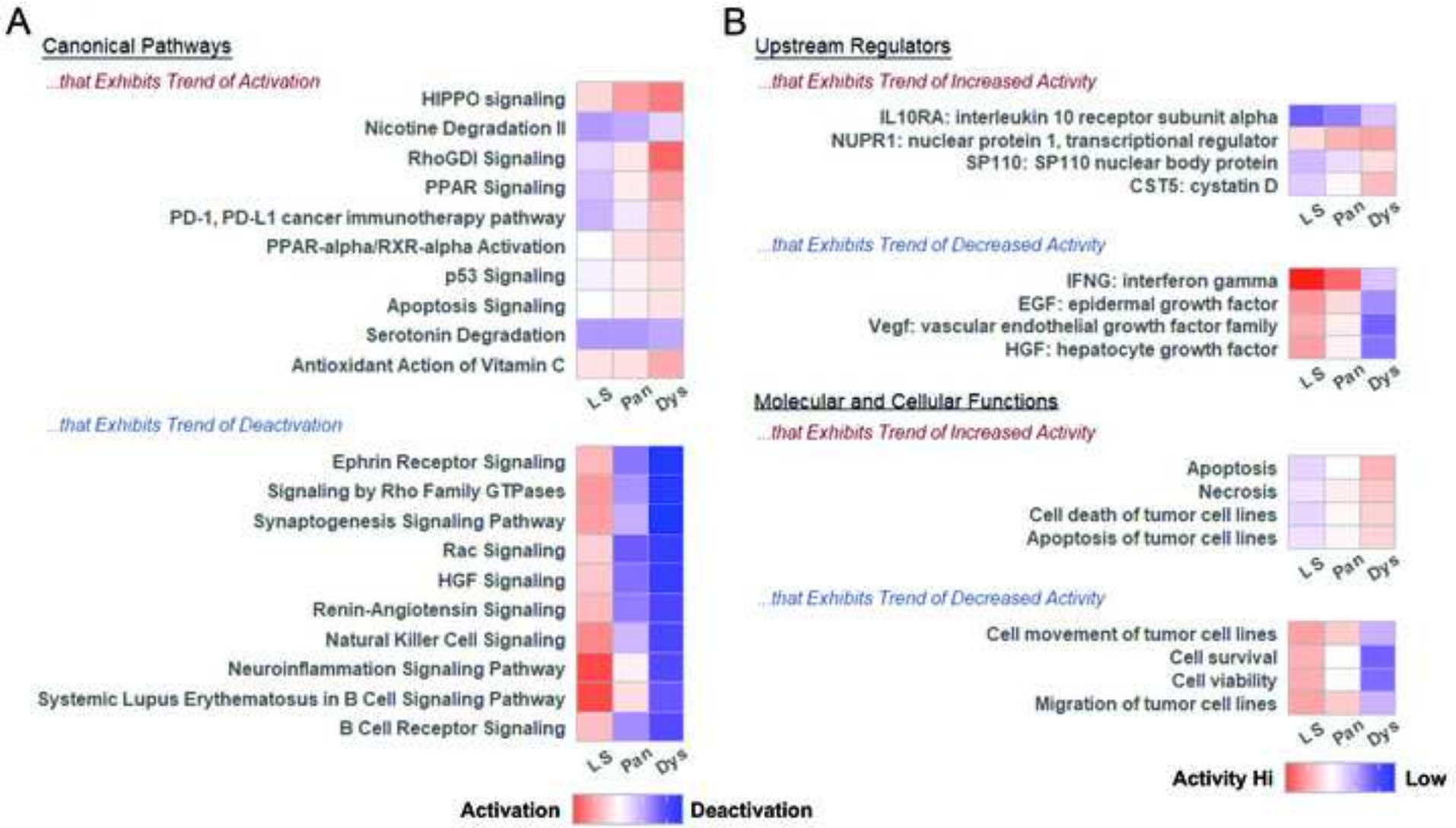

Figure 4

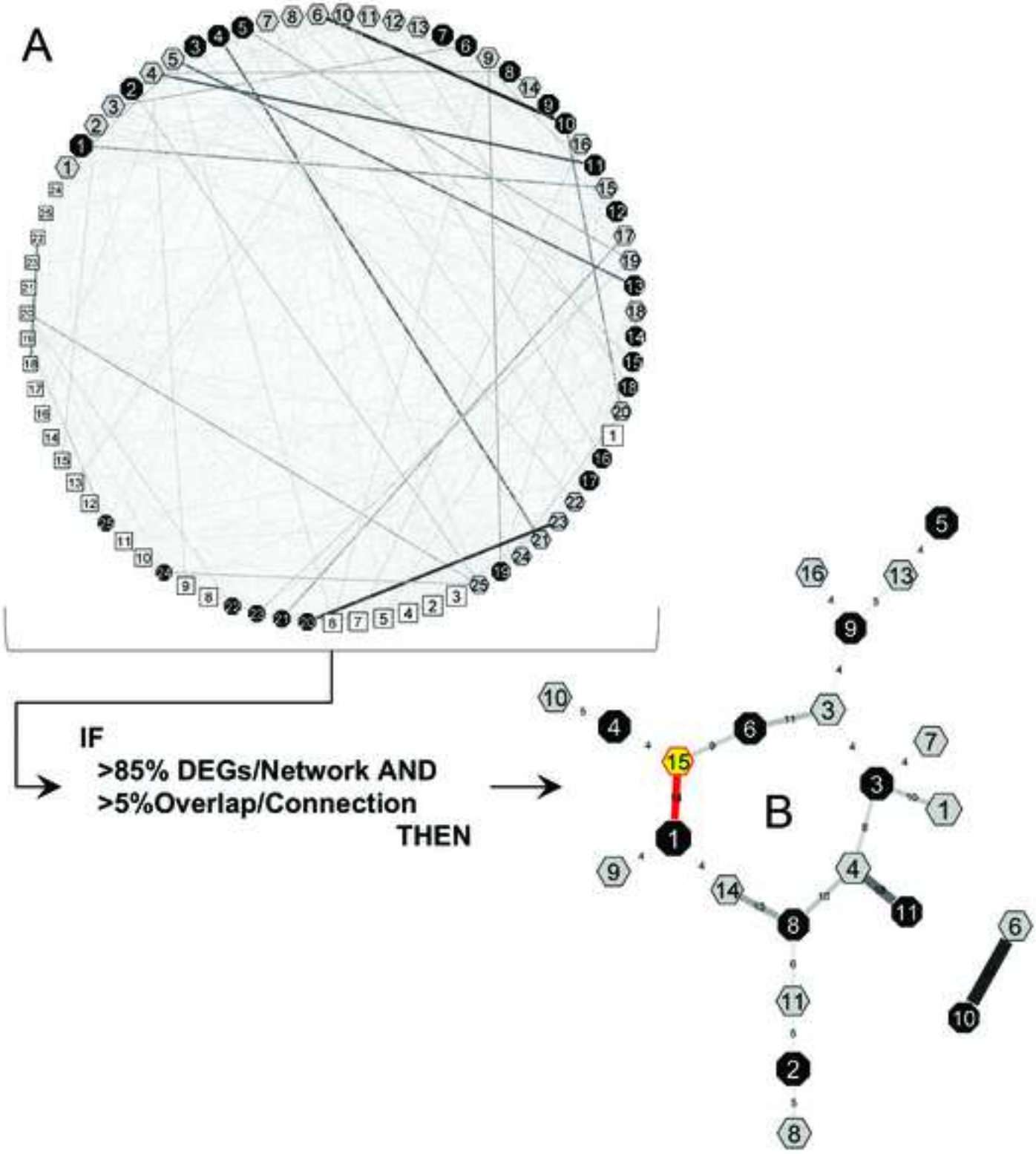

Figure 5 revised

Click here to access/download;Image;Figure 5v2.tif

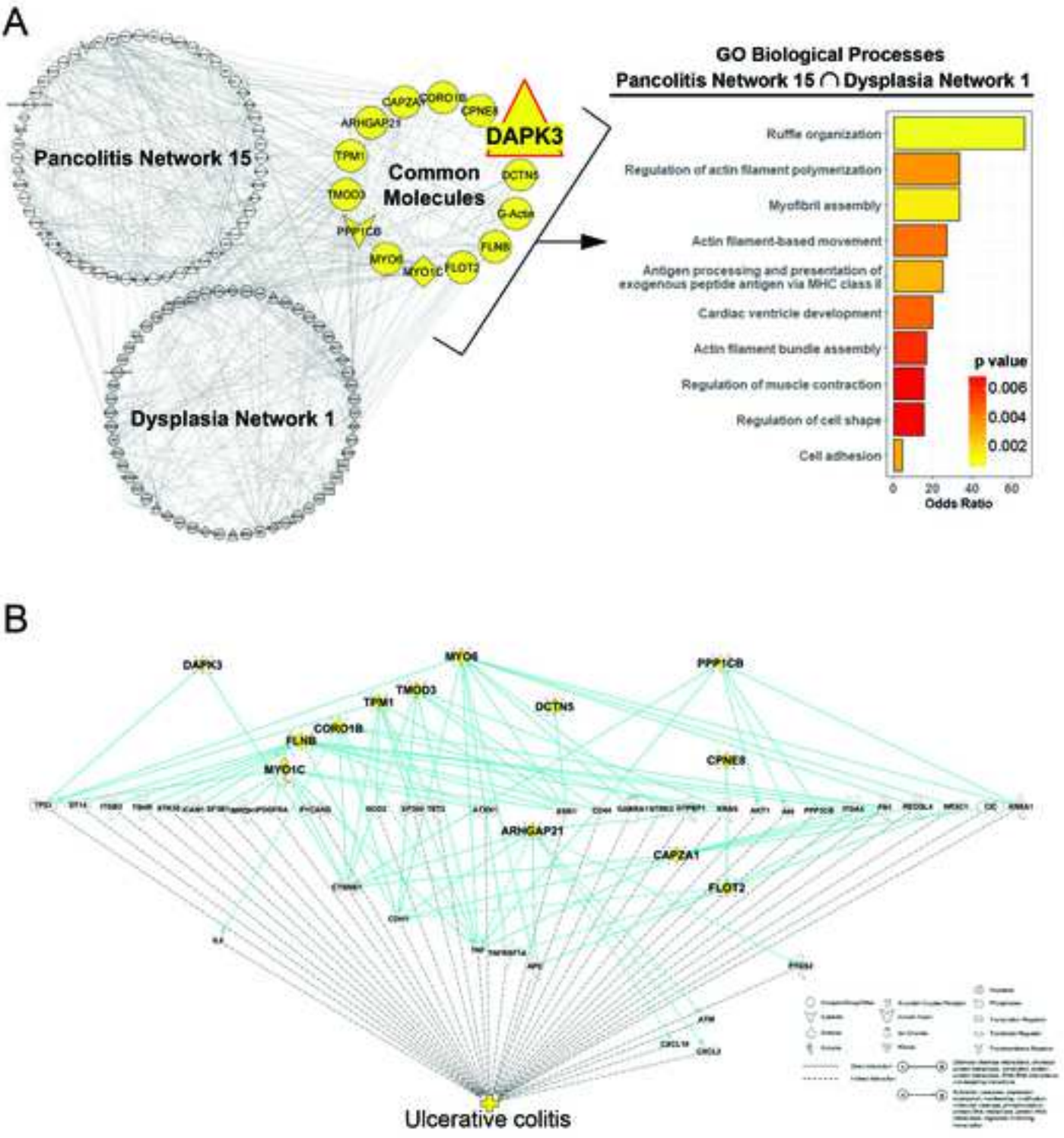

Figure 6

Click here to access/download;Image;Figure 6.tif